Journal of Radioanalytical and Nuclear Chemistry (2025) 334:3227–3240
https://doi.org/10.1007/s10967-025-10085-3

Prompt gamma rays induced by fission neutrons on sodium, silicon, sulfur and potassium

Eric Mauerhofer[1] · Niklas Ophoven[1] · Zeljko Ilic[1,2] · Christian Stieghorst[3] · Zsolt Révay[3] · Iaroslav Meleshenkovskii[1] · Tsitohaina H. Randriamalala[1]

Received: 2 December 2024 / Accepted: 15 March 2025 / Published online: 10 April 2025

Abstract
Prompt gamma rays produced during irradiation of sodium, silicon, sulfur and potassium with fission neutrons were measured with the FaNGaS instrument at Heinz-Maier-Leibnitz Zentrum. Relative intensities and production cross sections of 100 gamma lines (19 for sodium, 13 for silicon, 20 for sulfur and 48 for potassium) are presented and evaluated in comparison with existing literature data. Furthermore, the detection limits of sodium, silicon, sulfur and potassium were determined for a counting time of 12 h as 0.1, 0.6, 1 and 4 mg, respectively.

Keywords Fission neutrons · Sodium · Silicon · Sulfur · Potassium · Cross section · Detection limits

Introduction

FaNGaS (Fast Neutron induced Gamma-ray Spectrometry) is a new and worldwide unique instrument [1–3] operated at MLZ (Heinz Maier-Leibnitz Zentrum), which uses the powerful beam of fission neutrons provided by the SR10 (Strahlrohr 10) beam tube of FRM II (Forschungs-Neutronenquelle Heinz Maier Leibnitz) to perform nondestructive elemental analysis of large and thick items. Small and thin samples can also be investigated for example for nuclear data measurements. This analytical technique called "Prompt Gamma Analysis based on Inelastic Neutron Scattering" (PGAINS) is based on the measurement of isotope-specific prompt gamma rays induced by inelastic scattering of fission neutrons i.e. (n,n´γ) reactions, even in some cases gammas from (n,pγ)- or (n,$\alpha\gamma$)-reactions can be detected. The fission neutrons are generated by the thermal neutron-induced fission of ^{235}U in a uranium converter (93% of ^{235}U) plunged into the D_2O moderator of FRM II. After passing through various filters and collimators they are extracted into the MEDAPP (Medical Application) irradiation bunker. The size of the fission neutron beam is typically 6×6 cm^2 and can be adapted with the multi leaf collimator of MEDAPP. The fission neutron flux at sample position is 1.13×10^8 cm^{-2} s^{-1} and the average neutron energy is about 2.2 MeV. Gamma radiation is detected with a n-type high purity germanium (HPGe) detector of 50% relative efficiency, electromechanically cooled and positioned perpendicular to the neutron beam. The detector is protected against neutron and gamma background with a shielding made of lead-copper (Pb99.94 Cu) and borated (20% B_2O_3) polyethylene [3].

The use of PGAINS for chemical analysis requires reliable and accurate knowledge on the energies and production cross-sections of the gamma rays emitted by the aforementioned reactions. While the gamma-ray energies are generally well known and compiled, for example in NuDat 3.0 [4], a modern and comprehensive compilation of gamma-ray production cross sections for fission-neutrons induced reactions like (n,n´γ), (n,pγ) and (n,$\alpha\gamma$) are missing. Until now, the only available and useful database is the "Atlas of Gamma-ray spectra from the Inelastic Scattering of Reactor Fast Neutrons" published by Demidov et al. in 1978 [5]. This Atlas contains the relative intensities of 7375 prompt gamma rays for 76 natural and 29 isotopically-enriched elements, induced by fast neutrons with an average energy of 0.6 MeV and measured at an angle of 90° with respect to the neutron beam. Based on the data provided in [5] a valuable relational

✉ Eric Mauerhofer
e.mauerhofer@fz-juelich.de

[1] Jülich Centre for Neutron Science, Forschungszentrum Jülich GmbH, 52425 Jülich, Germany

[2] Lehrstuhl für Experimentalphysik IVc, RWTH Aachen University, 52056 Aachen, Germany

[3] Heinz Maier-Leibnitz Zentrum (MLZ), Technische Universität München, 85747 Garching, Germany

database was recently developed [6]. In the frame of the development of the PGAINS technique, the fission-neutron spectrum-averaged partial gamma-ray cross sections were measured for 15 elements (C, O, Al, Cl, Ca, Ti, Fe, Ni, Cu, Zr, In, La, Ce, Pr, Tb) with the FaNGaS instrument at FRM II [2, 3, 7–12]. The gamma-ray intensities were found to be consistent with the values determined in [5].

In this work, we report on the production cross sections of the prompt gamma rays induced by the interaction of fission neutrons with sodium, silicon, sulfur and potassium by irradiating sodium carbonate (Na_2CO_3), silica (SiO_2), plastic sulfur (S) and a potassium carbonate (K_2CO_3) sample, respectively. The relative intensities of the gamma rays are compared with those listed in [5]. Additionally, the partial cross section of the carbon and oxygen lines are compared with the values obtained from our previous measurements on $CaCO_3$ [3] and PVC [9]. Furthermore, the elemental detection limits for sodium, silicon, sulfur and potassium are given.

Experimental

Gammas emitted from the interaction of fission neutrons on Na_2CO_3 (2.875 g), SiO_2 (1.665 g), K_2CO_3 (1.863 g) powder samples and on a plastic sulfur disc (∅ = 8 mm, e = 3 mm, 0.317 g) were measured with the FaNGaS instrument whose specifications are given in [3]. The powder samples were sealed into polyethylene bags and their thickness was estimated to be 2 mm. The sulfur sample was contained in a fluorinated ethylene-propylene copolymer (FEP) bag. The samples were rotated by an angle of 45° regarding to the neutron beam direction. The thermal, epithermal and fast neutron flux at sample position was $(3.2 \pm 1.3) \times 10^3$ cm^{-2} s^{-1} (10^{-10} MeV < E_n < 1.42 10^{-7} MeV), $(2.9 \pm 0.8) \times 10^6$ cm^{-2} s^{-1} (1.42 10^{-7} MeV < E_n < 0.06 MeV) and $(1.13 \pm 0.04) \times 10^8$ cm^{-2} s^{-1} (0.06 < E_n < 20 MeV) [10]. The neutron spectrum average energy was 2.18 ± 0.06 MeV. The irradiation time was 6.3 h for Na_2CO_3, 10.1 h for SiO_2, 12.7 h for S and 6.9 h for K_2CO_3. The gamma-ray spectra were acquired for 4.4, 8.1, 11.2 and 5.6 h (live times), respectively. The measurements were done at an angle of 90° between neutron beam axis and detector. The sample-to-detector distance was 67 cm. The analysis of the spectra was performed with the software HYPERMET-PC [13]. The identification and correction of background interferences was achieved using previous beam background analysis [2]. Interferences from single (SE) and double (DE) escape peaks were corrected using the method developed in [9]. The spectra of the Na_2CO_3, SiO_2, S and K_2CO_3 are shown together with the beam background in Figs. 1, 2, 3 and 4, respectively. The count rates of background lines were observed to increase by a mean factor of 2.41 ± 0.49 for Na_2CO_3, 1.73 ± 0.28 for SiO_2, 1.17 ± 0.09 for S and 1.82 ± 0.27 for K_2CO_3 due to the scattering of neutrons towards the HPGe-detector. These factors were considered in the correction of background interferences. The identification of the gamma rays issued from inelastic scattering as well as from capture of fission neutrons was supported by the database NuDat 3.0 [4] and the nuclear data provided in [14–21]. In the case of (n,γ) reactions the PGNAA database [22] was used.

Method

The net peak area $\boldsymbol{P_{E\gamma}}$ of a prompt or a delayed gamma ray of energy E_γ can be expressed by:

$$P_{E\gamma} = \frac{m}{M} N_A h\, \varepsilon_{E\gamma} \left\langle \sigma_{E\gamma} \right\rangle \Phi\, t_c f_n\, f_{E\gamma}\, g\left(t_b, t_c, t_{1/2}\right) \tag{1}$$

where m (g) is the amount of element, M (g mol^{-1}) the molar mass of the element, N_A the Avogadro number, h the abundance of the isotope considered, $\boldsymbol{\varepsilon_{E\gamma}}$ the full-energy-peak efficiency, $\langle \boldsymbol{\sigma_{E\gamma}} \rangle$ (cm^2) the isotopic production cross section of the gamma-ray, $\boldsymbol{\Phi}$ (cm^{-2} s^{-1}) the neutron flux, $\boldsymbol{f_n}$ the neutron self-shielding factor and $\boldsymbol{f_{E\gamma}}$ the gamma-ray self-absorption factor. The term $\boldsymbol{g\left(t_b, t_c, t_{1/2}\right)}$ is equal to the counting live time $\boldsymbol{t_c}$(**s**) for a prompt gamma ray and can be given for a delayed gamma by:

$$g\left(t_b, t_c, t_{1/2}\right) = t_c - \frac{t_c \cdot t_{1/2}}{t_b \cdot \ln 2} \cdot \left(1 - e^{-\frac{\ln 2 \cdot t_b}{t_{1/2}}}\right) \tag{2}$$

with $\boldsymbol{t_b}$ (s) the irradiation (real) time and $\boldsymbol{t_{1/2}}$ (s) the half-live of the activation product. The relationship between the isotopic production cross section $\langle \boldsymbol{\sigma_{E\gamma}} \rangle$ and the effective cross section $\langle \boldsymbol{\sigma} \rangle$ of the considered reaction is:

$$\sigma_{E\gamma} = I_{E\gamma} \cdot \sigma \tag{3}$$

where $\boldsymbol{I_{E\gamma}}$ is the intensity of the gamma ray taken into account the contribution of internal conversion.

As the samples were thin and gamma rays with energies above 300 keV were measured, corrections for absorption and multiple scattering of neutrons and for self-absorption of gammas were not considered, i.e. $\boldsymbol{f_n} \approx 1$, and $\boldsymbol{f_{E\gamma}} \approx 1$.

The intensity of the gamma rays of sodium, silicon, sulfur and potassium, respectively, were calculated relative to the element-specific reference gamma line used in [5]. The relationship between the determined intensities ($\boldsymbol{I_R}$) and the intensities ($\boldsymbol{I_{RD}}$) given in [5] was analyzed with the following semi-empirical function:

$$I_R = a \cdot \left(I_{RD}\right)^b \tag{4}$$

with $\boldsymbol{a}$ and $\boldsymbol{b}$ the coefficients returned by the fit of the data. In addition, the agreement between the two sets of data was

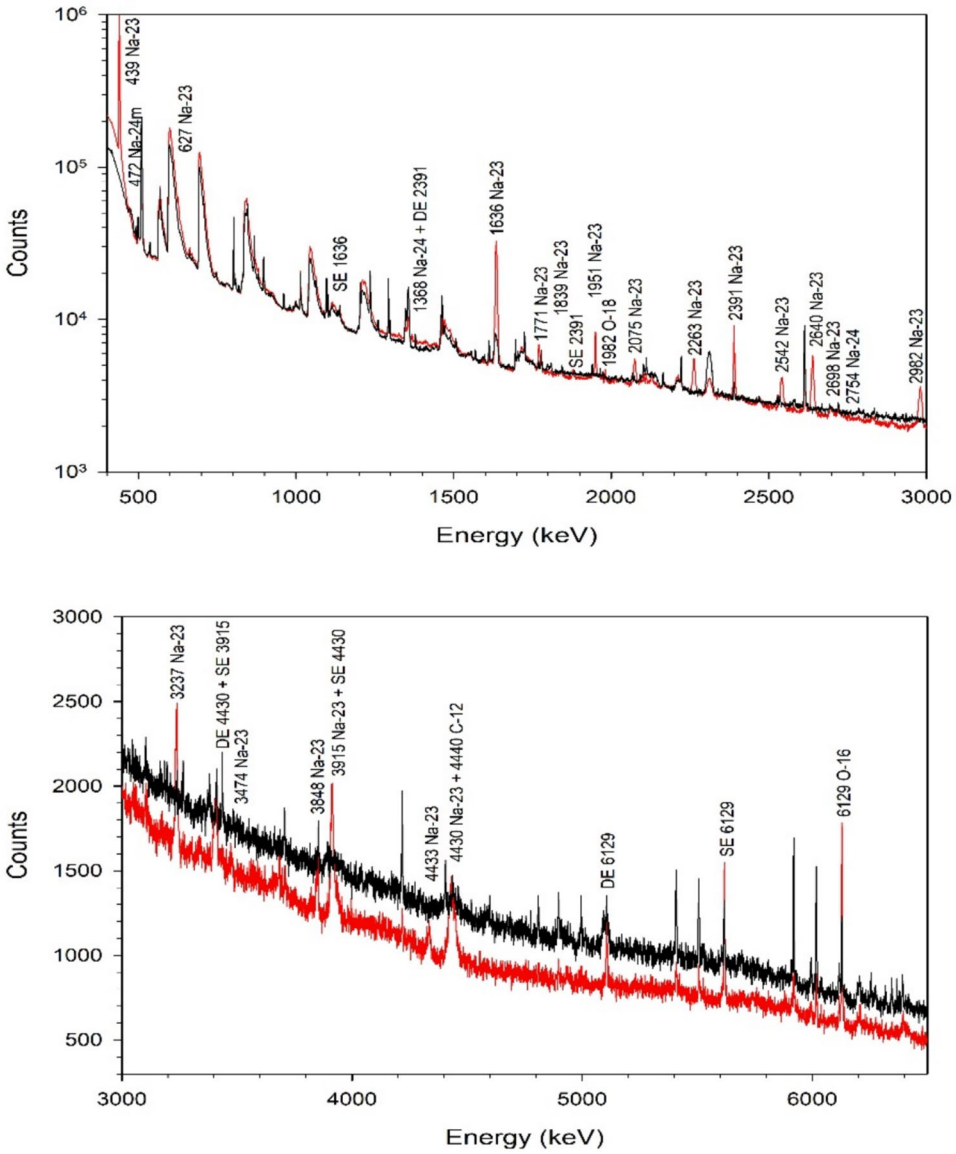

Fig. 1 Gamma-ray spectra in the energy range 400–6500 keV recorded during 15,819 s for Na_2CO_3 (red) and 51,506 s for the beam background (black). SE: single escape peak, DE: double escape peak. (Color figure online)

deduced from the distribution of the residuals in unit of standard deviation [σ], calculated, as:

$$r = \frac{I_R - I_{RD}}{\sqrt{\left(s_{I_R}\right)^2 + \left(s_{I_{RD}}\right)^2}} \tag{5}$$

where s is the absolute uncertainty of the intensity.

The fission-neutron spectrum-averaged isotopic cross sections for gamma-ray production, i.e. $\langle \sigma_{E\gamma} \rangle$-values, were calculated by Eq. (1) with a fast neutron flux of $(1.13 \pm 0.04) \times 10^8$ cm^{-2} s^{-1}.

Gamma rays of sodium

Nineteen prompt gamma lines issued from the inelastic scattering of fission neutrons with sodium were identified (see Table 1). Contributions from the ^{23}Na(n,p)^{23}Ne and ^{23}Na(n,α)^{20}F reactions were neglected due to their lower cross sections with regard to the ^{23}Na(n,n´)^{23}Na reaction. With the exception of the 439.4-keV line, all lines show a Doppler broadening because the nuclear lifetime of their respective excited states is smaller (≈ fs [4]) than the time needed by the recoiling nucleus to come to rest. Compared to

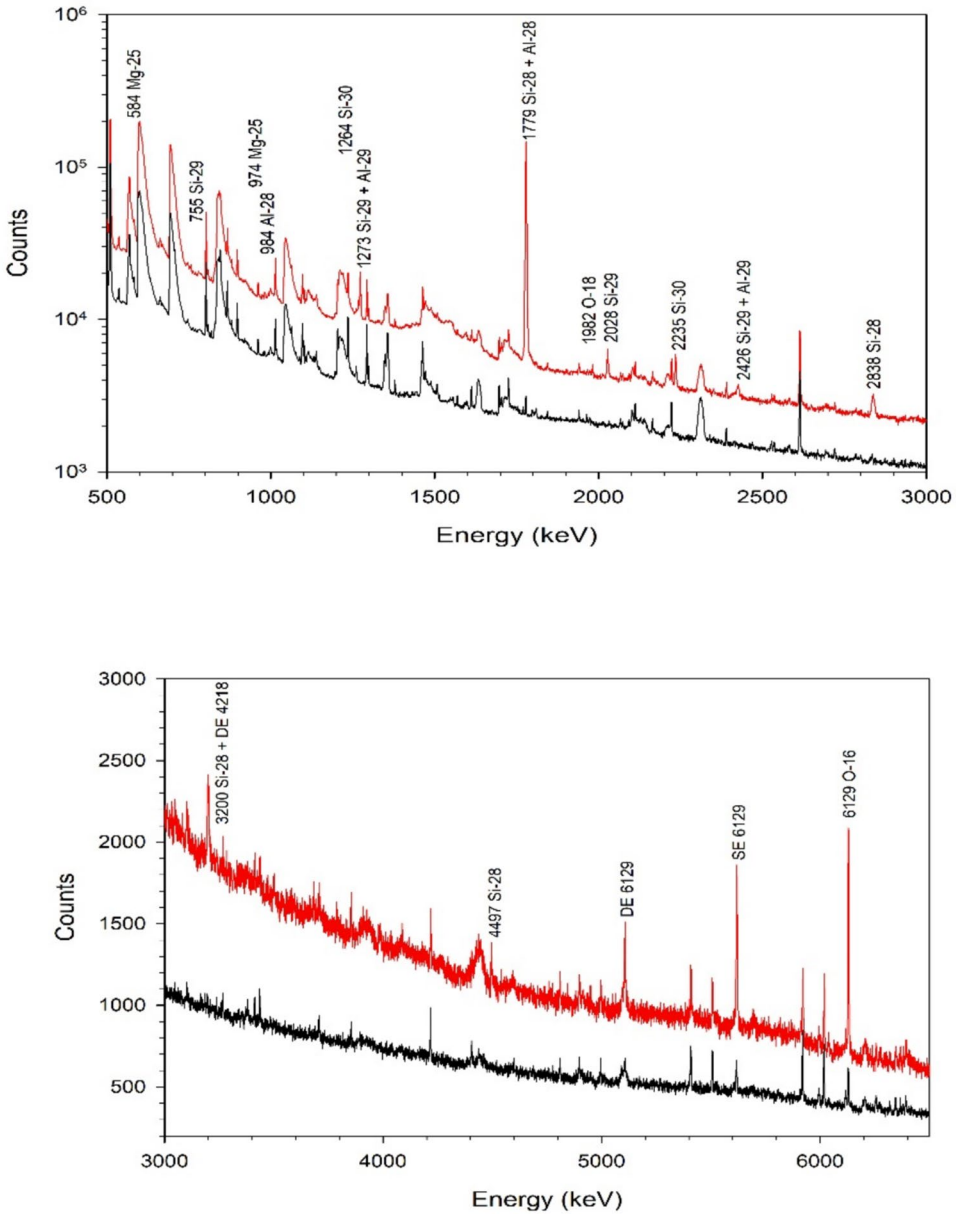

Fig. 2 Gamma-ray spectra in the energy range 400–6500 keV recorded during 29,210 s for SiO_2 (red) and 51,506 s for the beam background (black). SE: single escape peak, DE: double escape peak. (Color figure online)

the work of Demidov [5], one additional line at 3474.2 keV was detected. This line is reported together with the 1839.1-keV line in the database Nudat 3.0 [4], both deexciting from the 3914.6-keV level.

The relative intensities of the lines were calculated using the 439-keV line as reference (100%). They are presented together with the values determined in [5] in Table 1. The correlation between the two sets of intensities is shown in Fig. 5 and is described by Eq. (4) with $a = 0.96 \pm 0.07$ and $b = 1.15 \pm 0.07$. The residuals R calculated by means of Eq. (5) are plotted in the form of a histogram in Fig. 5. The fit with a Gaussian shows an agreement between the two set of data at the 0.6σ level indicating a good consistency. The shift of the Gaussian centroid by -0.07 ± 0.05 suggests no relevant systematic effect. The $\langle \sigma_{E\gamma} \rangle$-values are given in column 4 of Table 1.

Additionally, the 472.2-keV ($I_{E_\gamma} = 100\%$) line of ^{24m}Na ($T_{1/2} = 20.2$ ms) and the 1368.6-keV ($I_{E_\gamma} = 100\%$) and 2754.0-keV ($I_{E_\gamma} = 99.94\%$) lines of ^{24}Na ($T_{1/2} = 14.96$ h) induced by neutron capture on ^{23}Na were well observed in the spectrum with counts i.e. $P_{E_\gamma}/\varepsilon_{E_\gamma}$-values of $(67 \pm 10)\ 10^6$, $(14 \pm 2)\ 10^6$ and $(13 \pm 3)\ 10^6$, respectively. The 1368-keV line was corrected for the contribution of the double escape peak of the 2390-keV line that corresponds to $53.2 \pm 0.6\%$ of the total counts. By means of Eq. (1) we calculate effective cross sections of 1.13 ± 0.17 mb and 1.70 ± 0.09 mb for the production of ^{24m}Na and $^{24\ m+g}$Na, respectively. The

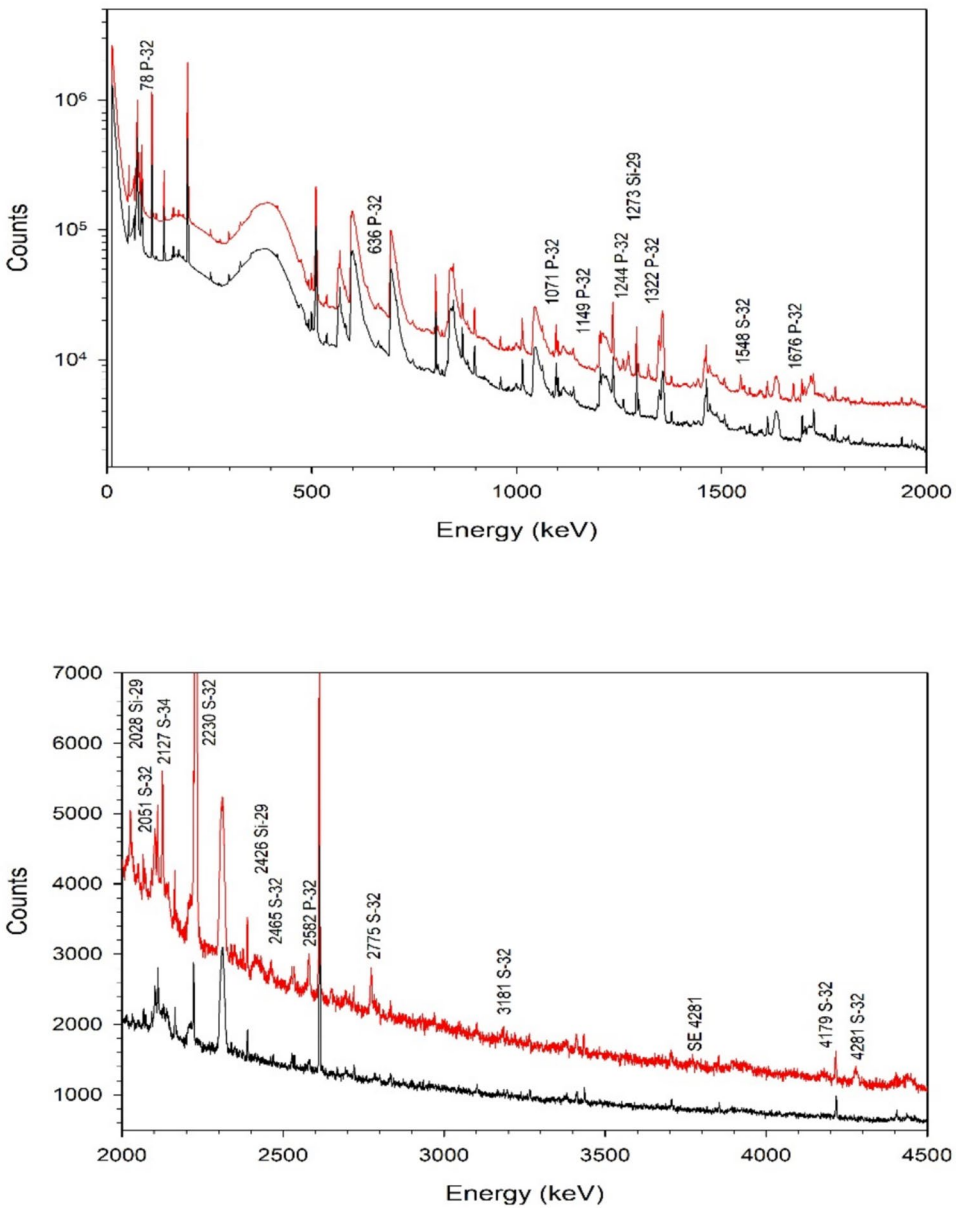

Fig. 3 Gamma-ray spectra in the energy range 0–4500 keV recorded during 40,457 s for S (red) and 51,506 s for the beam background (black). SE: single escape peak. (Color figure online)

difference of the two values leads to an effective cross section of 0.57 ± 0.19 mb for the direct production of ^{24g}Na. This value agrees well with the value of 0.58 ± 0.14 mb determined from the convolution of the ^{23}Na(n, γ)^{24g}Na-reaction cross sections taken from the ENDF/B-VIII.0 library [23] with our neutron energy spectrum using the NJOY Nuclear Data Processing System (Version 2016) [24, 25]. It is higher than the cross section of 0.28 mb evaluated for a pure fission spectrum (kT = 1.35 MeV) [26] due a higher proportion of epithermal neutrons in our spectrum.

Gamma rays of silicon

Thirteen prompt gamma lines from the interaction of fission neutrons with silicon were identified, 4 associated to ^{28}Si(n,n′γ)^{28}Si-, 4 to ^{29}Si(n,n′γ)^{29}Si-,2 to ^{30}Si(n,n′γ)^{30}Si-, 1 to ^{28}Si(n,pγ)^{28}Al- and 2 to ^{28}Si(n,$\alpha\gamma$)^{25} Mg-reactions (see Table 2). All the lines given in [5] were detected. The 1778.9-keV ($I_{E_\gamma} = 100\%$) γ-ray of ^{28}Al ($T_{1/2} = 2.24$ min) produced by the ^{28}Si(n,p)^{28}Al reaction and the 1273.4-keV ($I_{E_\gamma} = 90.6\%$) and 2425.9-keV ($I_{E_\gamma} = 5.7\%$) γ-rays, respectively, induced by the ^{29}Si(n,p)^{29}Al reaction were found to interfere with the prompt gamma lines of silicon of same energy. Their contributions to the count rates were evaluated to $4.0 \pm 0.2\%$, $2.1 \pm 0.1\%$ and $1.43 \pm 0.06\%$, respectively, and the intensities of the corresponding lines were corrected accordingly.

The intensities of the lines calculated relative to the 1779-keV line (100%) are given with the values

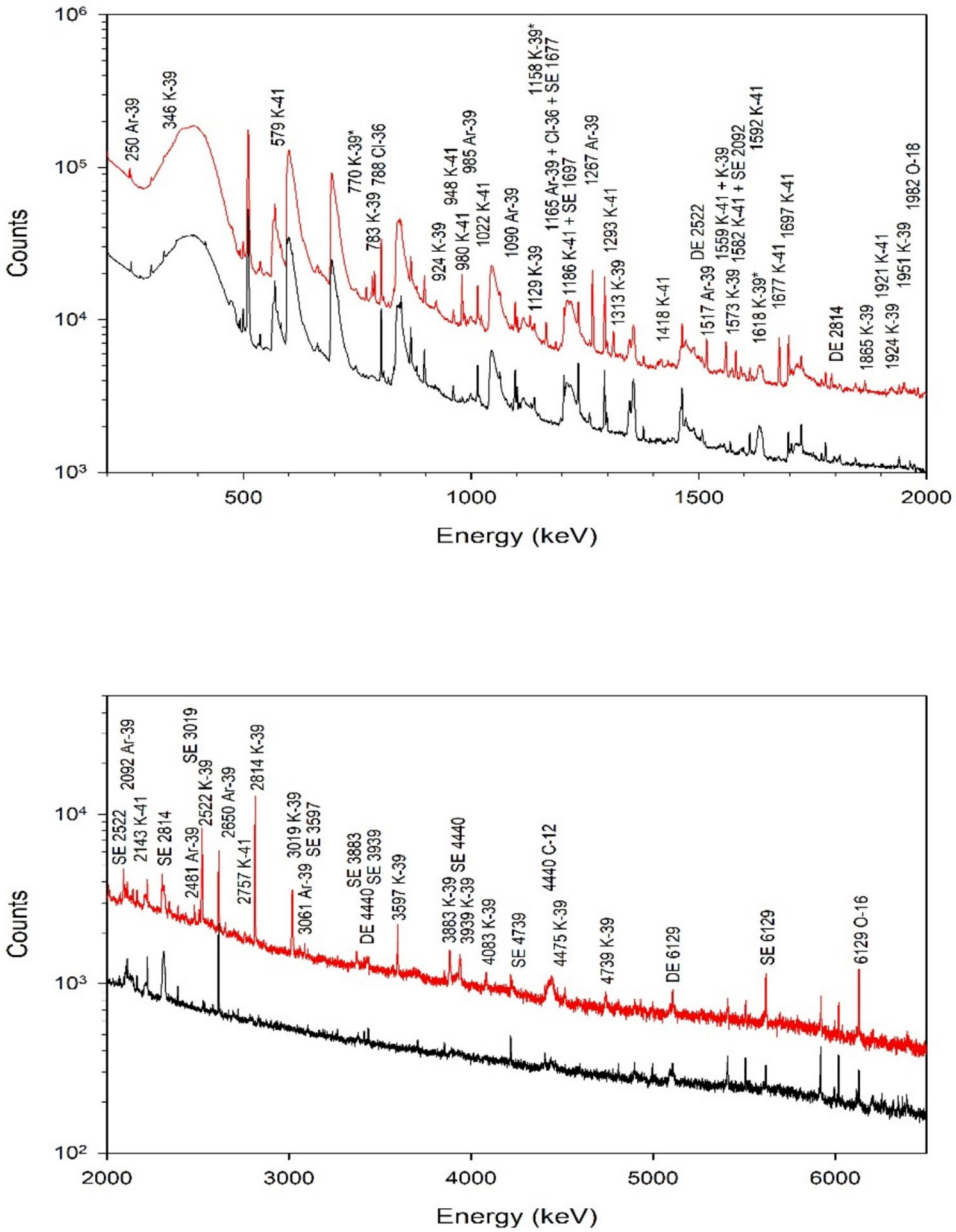

Fig. 4 Gamma-ray spectra in the energy range 200–6500 keV recorded during 20,092 s for K_2CO_3 (red) and 51,506 s for the beam background (black). SE: single escape peak. (Color figure online)

determined in [5] in Table 2. The correlation between the two data sets and the histogram of the residuals are shown in Fig. 6. The relationship between the data is expressed by means of Eq. (4) with $a = 0.73 \pm 0.20$ and $b = 1.24 \pm 0.07$. The fit of the residuals with a Gaussian indicates a good agreement at the 0.9σ level. However, the Gaussian centroid is shifted by -1.18 ± 0.10 pointing out a systematic effect that we associate to the lines at 584.6, 974.9, 983.6, 1264.1 and 3199.7 keV. For these lines, the intensities reported in [5] are higher by a factor of about 2 than the ones measured in our work and thus we can assume that they were not corrected for possible interferences (see footnotes of Table 2). The $\langle \sigma_{E\gamma} \rangle$-values are given in column 4 of Table 2.

Gamma rays of sulfur

Twenty prompt gamma lines from the interaction of fission neutrons with sulfur were measured, 9 related to (n,n´γ)-, 8 to ^{32}S(n,pγ)^{32}P- and 3 to ^{32}S(n,$\alpha\gamma$)^{29}Si-reactions (see Table 3). From the 9 (n,n´γ)-reactions 8 lines were assigned to ^{32}S and 1 to ^{34}S. All lines given in [5] were detected except the lines of ^{32}P at 2097.5 keV from the 2177.2-keV level [4] and 2151.6 keV from the 2229.7-keV level [4]. It was not possible to observe the 2097.5-keV line due to interferences of the background lines at 2098.0 keV (^{74}Ge) and 2097.3 keV (^{208}Pb) induced by inelastic scattering of fast neutrons with the HPGe detector and the surrounding lead shielding. The weak line at

Table 1 Prompt gamma rays of ^{23}Na induced by inelastic scattering of fission neutrons

This work				From Demidov atlas [5]		R
E_γ (keV)	$P_{E_\gamma}/\varepsilon_{E_\gamma}$ ($\times 10^{-8}$) (Count)	I_R (relative) (%)	σ_{E_γ} (mb)	E_γ (keV)	I_{RD} (relative) (%)	
439.41 ± 0.03	296 ± 9	100	507 ± 24	440.0 ± 0.2	100	–
626.83 ± 0.03	2.26 ± 0.09	0.76 ± 0.04	3.85 ± 0.20	627.6 ± 0.2	0.90 ± 0.15	− 0.90
1635.96 ± 0.06[a]	32.4 ± 1.3	10.9 ± 0.5	55 ± 3	1635.8 ± 0.2	8.6 ± 0.8	2.43
1771.34 ± 0.11[a]	2.06 ± 0.13	0.69 ± 0.05	3.50 ± 0.25	1772.50 ± 0.10	0.80 ± 0.15	− 0.69
1838.91 ± 0.37	0.15 ± 0.03	0.05 ± 0.01	0.25 ± 0.05	1839.30 ± 0.15	0.10 ± 0.05	− 0.98
1950.70 ± 0.08	2.92 ± 0.41	0.98 ± 0.14	4.97 ± 0.72	1951.0 ± 0.4	1.10 ± 0.3	− 0.36
2074.96 ± 0.08[a]	2.88 ± 0.25	0.97 ± 0.09	4.92 ± 0.46	2075.3 ± 0.6	0.85 ± 0.10	0.89
2263.17 ± 0.09	4.21 ± 0.39	1.42 ± 0.14	7.20 ± 0.71	2263.2 ± 0.5	1.2 ± 0.2	0.90
2390.70 ± 0.09[a]	5.04 ± 0.37	1.70 ± 0.13	8.62 ± 0.70	2390.6 ± 0.5	1.8 ± 0.2	− 0.42
2541.57 ± 0.10[a]	3.48 ± 0.29	1.17 ± 0.17	5.93 ± 0.54	2542.0 ± 0.5	1.1 ± 0.2	0.38
2639.85 ± 0.10	6.34 ± 0.57	2.14 ± 0.20	10.8 ± 1.0	2640.1 ± 0.5	2.0 ± 0.4	0.31
2698.14 ± 0.11[a]	0.60 ± 0.08	0.20 ± 0.03	1.01 ± 0.14	2698.1 ± 0.1	0.15 ± 0.05	0.93
2981.77 ± 0.09	4.53 ± 0.46	1.53 ± 0.16	7.76 ± 0.83	2981.7 ± 0.1	1.4 ± 0.2	0.50
3237.48 ± 0.10[a]	2.26 ± 0.26	0.76 ± 0.09	3.85 ± 0.46	3238.20 ± 0.12	0.90 ± 0.15	− 0.80
3474.20 ± 0.38	0.16 ± 0.03	0.05 ± 0.01	0.25 ± 0.05	–	–	–
3848.10 ± 0.37	0.27 ± 0.04	0.09 ± 0.01	0.46 ± 0.07	3848.20 ± 0.15	0.20 ± 0.08	− 1.36
3914.52 ± 0.15[b]	1.10 ± 0.13	0.37 ± 0.04	1.87 ± 0.23	3914.80 ± 0.18	0.45 ± 0.15	− 0.55
4333.35 ± 0.19	0.84 ± 0.13	0.28 ± 0.04	1.42 ± 0.22	4334 ± 2	0.40 ± 0.10	− 1.11
4434.50 ± 0.18[c]	1.50 ± 0.29	0.50 ± 0.10	2.53 ± 0.48	4430.40 ± 0.12	0.35 ± 0.12	0.96

E_γ is the gamma-ray energy, $P_{E_\gamma}/\varepsilon_{E_\gamma}$ the net count in the gamma-ray peak divided by the full-energy-peak efficiency and the gamma-ray self-absorption factor,I_R the relative intensity of the gamma-ray and $\langle \sigma_{E\gamma} \rangle$ the fast neutron spectrum averaged isotopic cross section for gamma ray production at an angle of 90° between neutron beam and detector determined with Eq. (1). R is the residual calculated by means of Eq. (6). The uncertainty for $P_{E\gamma}(90°)/(\varepsilon_{E\gamma} \cdot f_{E\gamma})$ is calculated from the uncertainty of the net counts of the lines $P_{E\gamma}(90°)$ and the uncertainty of the full-energy peak efficiency $\varepsilon_{E\gamma}$ (3%) The uncertainty for $<\sigma_{E\gamma}(90°)>$ is calculated from the uncertainty of $P_{E\gamma}(90°)/(\varepsilon_{E\gamma} \cdot f_{E\gamma})$ and the uncertainty of the fast neutron flux (3.5%)

[a]Corrected for the contribution of the 1635-keV (^{14}N) background line (2.2% of total counts)

[b]Corrected for the contribution of single escape peak of 4434 keV (66.3% of total counts)

[c]Corrected for the interference of 4441 keV from ^{12}C(n,n´)^{12}C using a partial cross section of 13.3 ± 1.9 mb [9]

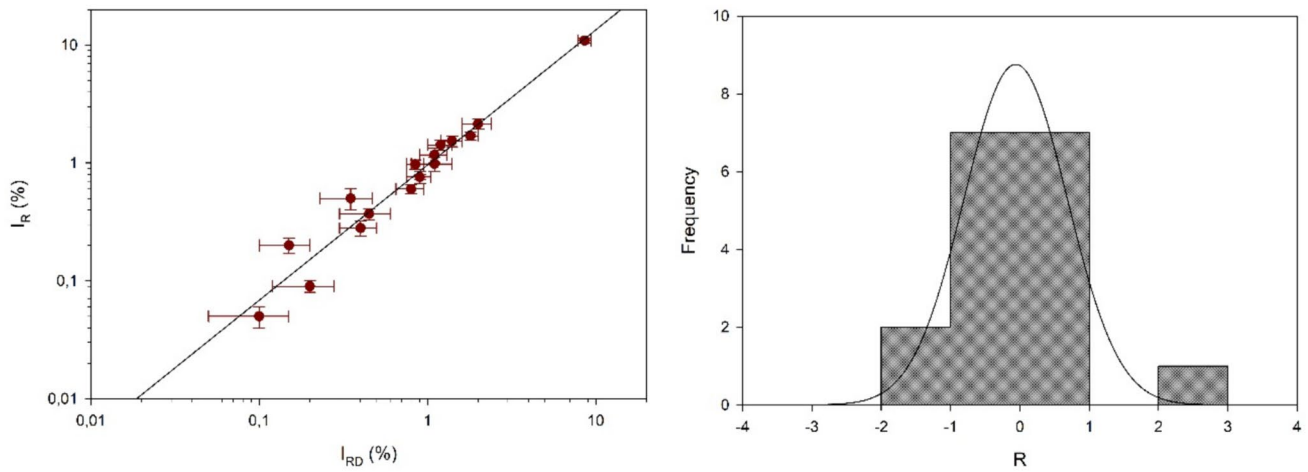

Fig. 5 Comparison of the relative intensities of the prompt gamma rays induced by inelastic scattering of fast neutrons on sodium obtained in this work with the data tabulated in the Demidov Atlas [5]. Left figure: linear relationship; the solid line represents the fit of the data with Eq. (4). Right figure: histogram of the residuals R in units of standard deviation [σ] calculated with Eq. (5). The values of R are given in column 7 of Table 1. The solid line represents the fit of the data with a Gaussian

Table 2 Prompt gamma rays induced by fission neutrons on silicon

Reaction	This work				From Demidov Atlas [5]		R
	E_γ (keV)	$P_{E_\gamma}/\varepsilon_{E_\gamma}$ ($\times 10^8$) (Count)	I_R(relative) (%)	σ_{E_γ} (mb)	E_γ (keV)	I_{RD}(relative) (%)	
$^{28}Si(n,n'\gamma)^{28}Si$	1778.85 ± 0.07[a]	95 ± 3	100	189 ± 9	1778.8 ± 0.3	100	–
	2837.88 ± 0.10	2.24 ± 0.09	2.35 ± 0.12	4.45 ± 0.24	2837.9 ± 0.1	2.7 ± 0.3	− 1.08
	3199.74 ± 0.03[b]	0.45 ± 0.06	0.48 ± 0.07	0.90 ± 0.12	3199.90 ± 0.15[c]	1.0 ± 0.2	− 2.45
	4496.9 ± 0.3	0.65 ± 0.11	0.69 ± 0.12	1.30 ± 0.22	4496.30 ± 0.15	0.84 ± 0.30	− 0.46
$^{29}Si(n,n'\gamma)^{29}Si$	755.55 ± 0.04	0.58 ± 0.05	0.60 ± 0.06	22.5 ± 2.1	–	–	–
	1273.14 ± 0.05[d]	4.45 ± 0.15	4.67 ± 0.22	175 ± 8	1272.8 ± 0.4	4.2 ± 0.1	1.94
	2027.82 ± 0.09	1.67 ± 0.08	1.75 ± 0.10	65.5 ± 3.9	2027.9 ± 0.5	2.0 ± 0.4	− 0.60
	2425.9 ± 0.1[e]	0.68 ± 0.06	0.72 ± 0.07	26.9 ± 2.5	2425.2 ± 0.5	0.85 ± 0.20	− 0.61
$^{30}Si(n,n'\gamma)^{30}Si$	1264.09 ± 0.22	0.32 ± 0.04	0.34 ± 0.04	19.0 ± 2.5	1262.9 ± 0.8[f]	0.60 ± 0.20	− 1.27
	2235.08 ± 0.10	1.97 ± 0.10	2.07 ± 0.12	116 ± 7	2234.9 ± 0.5	2.4 ± 0.5	− 0.64
$^{28}Si(n,p\gamma)^{28}Al$	983.6 ± 0.4	0.19 ± 0.05	0.20 ± 0.06	0.38 ± 0.10	983.4 ± 0.5	0.35 ± 0.10	− 1.28
$^{28}Si(n,\alpha\gamma)^{25}$ Mg	584.4 ± 0.1	0.42 ± 0.03	0.44 ± 0.04	0.83 ± 0.07	584.6 ± 0.5[g]	0.85 ± 0.15	− 2.64
	973.9 ± 0.4	0.13 ± 0.05	0.14 ± 0.05	0.26 ± 0.10	974.8 ± 0.7[h]	0.25 ± 0.05	− 1.55

$E\gamma$ is the gamma-ray energy, $P_{E_\gamma}/\varepsilon_{E_\gamma}$ the net count in the gamma-ray peak divided by the full-energy-peak efficiency and the gamma-ray self-absorption factor,I_R the relative intensity of the gamma-ray and $\langle \sigma_{E\gamma} \rangle$ the fast neutron spectrum averaged isotopic cross section for gamma ray production at an angle of 90° between neutron beam and detector determined with Eq. (1). R is the residual calculated by means of Eq. (6). The uncertainty for $P_{E\gamma}(90°)/(\varepsilon_{E\gamma} \cdot f_{E\gamma})$ is calculated from the uncertainty of the net counts of the lines $P_{E\gamma}(90°)$ and the uncertainty of the full-energy peak efficiency $\varepsilon_{E\gamma}$ (3%) The uncertainty for $<\sigma_{E\gamma}(90°)>$ is calculated from the uncertainty of $P_{E\gamma}(90°)/(\varepsilon_{E\gamma} \cdot f_{E\gamma})$ and the uncertainty of the fast neutron flux (3.5%)

[a]Corrected for the contribution of the 1179-keV line of ^{28}Al produced by the $^{28}Si(n,p)^{28}Al$ reaction

[b]Corrected for the contribution of the double escape peak of the 4218-keV (^{56}Fe) background line (59.1% of total counts)

[c]Interference of the double escape peak of 4218 keV probably not considered

[d]Corrected from the contribution of the 1273-keV line of ^{29}Al produced by the $^{29}Si(n,p)^{29}Al$ reaction (2.1% of total counts)

[e]Corrected from the contribution of the 2426-keV line of ^{29}Al produced by the $^{29}Si(n,p)^{29}Al$ reaction (1.4% of total counts)

[f]Contains probably a contribution of the single escape peak of 1779 keV, not well resolved doublet

[g]Contains probably a contribution of the 583-keV (^{207}Pb) background line, not well resolved doublet

[h]Contains probably a contribution of the 977-keV (^{56}Fe) background line, not well resolved doublet

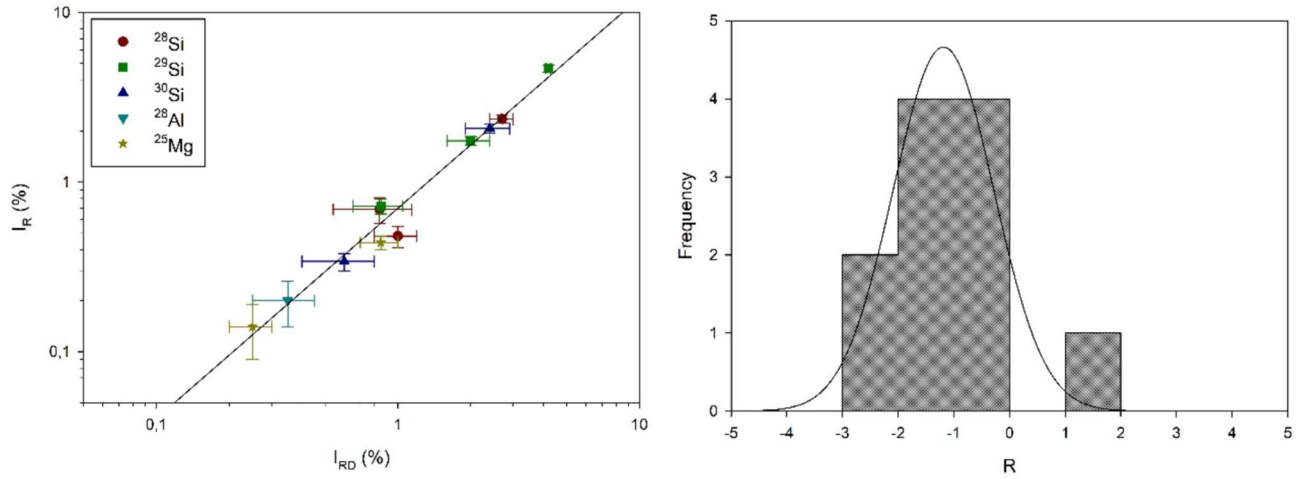

Fig. 6 Comparison of the relative intensities of the prompt gamma rays induced by fission neutrons on silicon obtained in this work with the data tabulated in the Demidov Atlas [5]. Left figure: linear relationship; the solid line represents the fit of the data with Eq. (4). Right figure: histogram of the residuals R in units of standard deviation [σ] calculated with Eq. (5). The values of R are given in column 7 of Table 1. The solid line represents the fit of the data with a Gaussian

Table 3 Prompt gamma rays induced by fission neutrons on sulfur

Reaction	This work				From Demidov atlas [5]		R
	E_γ (keV)	$P_{E_\gamma}/\varepsilon_{E_\gamma}$ ($\times 10^{-8}$) (Count)	I_R(relative) (%)	$\langle\sigma_{E\gamma}\rangle$ (mb)	E_γ (keV)	I_{RD}(relative) (%)	
^{32}S(n,n´γ)^{32}S	1547.81 ± 0.09	1.02 ± 0.05	4.96 ± 0.30	3.92 ± 0.24	1548.1 ± 0.3	3.0 ± 0.4	3.92
	2051.33 ± 0.35	0.12 ± 0.02	0.58 ± 0.12	0.46 ± 0.08	2052.0 ± 0.8	0.50 ± 0.10	0.51
	2230.48 ± 0.09	20.58 ± 0.70	100	79 ± 4	2230.2 ± 0.2	100	
	2465.43 ± 0.35	0.16 ± 0.03	0.78 ± 0.14	0.62 ± 0.12	2464.4 ± 0.14	1.4 ± 0.3	− 1.87
	2775.06 ± 0.09	0.68 ± 0.05	3.30 ± 0.29	2.61 ± 0.21	2776.1 ± 0.30	4.0 ± 0.4	− 1.42
	3180.64 ± 0.43	0.29 ± 0.08	1.41 ± 0.41	1.11 ± 0.31	3182.0 ± 0.12	1.2 ± 0.3	0.41
	4179 ± 1	0.63 ± 0.10	3.06 ± 0.50	2.42 ± 0.39			
	4281.41 ± 0.14	0.92 ± 0.08	4.47 ± 0.42	3.53 ± 0.33	4281.3 ± 0.15	4.0 ± 0.6	0.64
^{34}S(n,n´γ)^{34}S	2127.56 ± 0.08	1.30 ± 0.05	6.32 ± 0.39	114 ± 6	2127.5 ± 0.8	5.6 ± 0.5	1.13
^{32}S(n,pγ)^{32}P	78.93 ± 0.03	11.31 ± 0.51[a]	55 ± 3	44 ± 2	–	–	–
	636.2 ± 0.1	0.56 ± 0.07	2.72 ± 0.35	2.18 ± 0.28	636.2 ± 0.2	2.2 ± 0.4	0.98
	1070.98 ± 0.04	0.30 ± 0.05	1.46 ± 0.23	1.17 ± 0.20	1071.1 ± 0.2	1.6 ± 0.2	− 0.45
	1149.24 ± 0.05	0.09 ± 0.02	0.46 ± 0.11	0.35 ± 0.08	–	–	–
	1244.41 ± 0.13	0.32 ± 0.11	1.55 ± 0.18	1.24 ± 0.43	1245.2 ± 0.2	2.1 ± 0.3	− 1.57
	1322.58 ± 0.05	0.96 ± 0.06	4.66 ± 0.32	3.73 ± 0.27	1323.7 ± 0.4	3.0 ± 0.4	3.24
	1676.43 ± 0.07	1.02 ± 0.06	4.96 ± 0.32	3.97 ± 0.27	1676.9 ± 0.4	4.6 ± 0.4	0.70
	2581.8 ± 0.8	0.47 ± 0.09	2.28 ± 0.44	1.82 ± 0.35	–	–	–
^{32}S(n,αγ)^{29}Si	1273.52 ± 0.05	2.97 ± 0.11	14.43 ± 0.72	11.4 ± 0.6	1273.0 ± 0.2	13.0 ± 1	1.16
	2028.04 ± 0.17	0.65 ± 0.06	3.16 ± 0.33	2.50 ± 0.25	2028.4 ± 0.5[b]	6.2 ± 0.8	− 3.51
	2425.9 ± 1.9	0.32 ± 0.05	1.55 ± 0.25	1.23 ± 0.20			

E_γ is the gamma-ray energy, $P_{E_\gamma}/\varepsilon_{E_\gamma}$ the net count in the gamma-ray peak divided by the full-energy-peak efficiency and the gamma-ray self-absorption factor,I_R the relative intensity of the gamma-ray and $\langle\sigma_{E\gamma}\rangle$ the fast neutron spectrum averaged isotopic cross section for gamma ray production at an angle of 90° between neutron beam and detector determined with Eq. (1). R is the residual calculated by means of Eq. (6). The uncertainty for $P_{E\gamma}(90°)/(\varepsilon_{E\gamma}{\cdot}f_{E\gamma})$ is calculated from the uncertainty of the net counts of the lines $P_{E\gamma}(90°)$ and the uncertainty of the full-energy peak efficiency $\varepsilon_{E\gamma}$ (3%) The uncertainty for $<\sigma_{E\gamma}(90°)>$ is calculated from the uncertainty of $P_{E\gamma}(90°)/(\varepsilon_{E\gamma}{\cdot}f_{E\gamma})$ and the uncertainty of the fast neutron flux (3.5%)

[a]Corrected with a gamma self-absorption factor $f_{E_\gamma}=0.90$ calculated from a mass attenuation coefficient of 0.263 cm^2 g^{-1} [27], a sample density of 1.92 g cm^{-3} and an effective sample thickness of 4.2 mm

[b]Contains probably a contribution of the of the single escape peaks of 2536 keV (^{208}Pb) background line, not well resolved doublet

2151.6 keV was not detected due to the high background at the corresponding energy. Additional lines, which are listed in NuDat 3.0, were identified in our spectrum at 4179 keV for ^{32}S, 78.9, 1149.2 and 2581.8 keV for ^{32}P and 2425.9 keV for ^{29}Si.

The relative intensities of the lines were calculated using the 2230-keV line as reference (100%) and are compared with the values determined in [5] in Table 3. As shown in Fig. 7, the measured intensities in this work agree well with those determined in [5]. The relationship between the intensities is expressed by means of Eq. (4) with $a = 1.02 \pm 0.16$ and $b = 0.99 \pm 0.12$. The fit of the residuals with a Gaussian shows an agreement between the data at the 1.5σ level indicating a good consistency. The shift of the centroid by 0.59 ± 0.06 indicates a possible systematic effect. The $\langle\sigma_{E\gamma}\rangle$-values are given in column 4 of Table 3.

Gamma rays of potassium

Forty eight prompt gamma lines from the interaction of fission neutrons with potassium were measured, 19 related to ^{39}K(n,n′γ)^{39}K-, 15 to ^{41}K(n,n′γ)^{41}K-, 12 to ^{39}K(n,pγ)^{39}Ar- and 2 to ^{39}K(n,αγ)^{36}Cl-reactions (see Table 4). All lines given in [5] were detected and assigned to corresponding isotopes except the lines at 1106.9 and 3369.5 keV, which are not reported in NuDat 3.0 [4]. Further lines listed in NuDat 3.0 [4] were detected:

- 1573.6, 1924.2, 1951.4, 4474.9 and 4739.2 keV for ^{39}K
- 947.6, 1186.1, 1418.6, 1592.5, 1920.8, 2143.5 and 2756.7 keV for ^{41}K
- 985.5, 1090.6, 2433.8, 2650.0 and3061.7 keV for ^{39}Ar

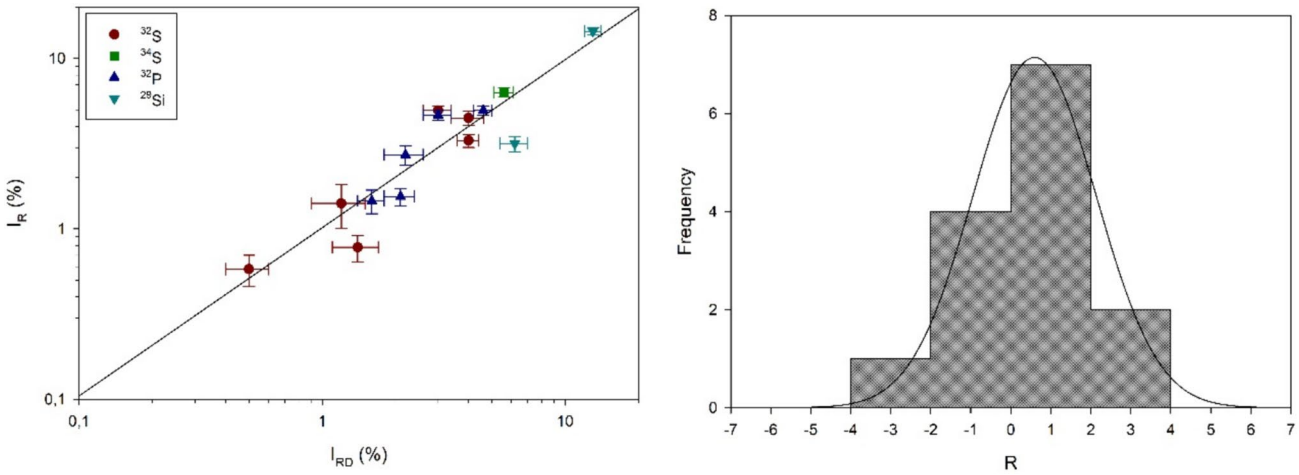

Fig. 7 Comparison of the relative intensities of the prompt gamma rays induced by fission neutrons on sulfur obtained in this work with the data tabulated in the Demidov Atlas [5]. Left figure: linear relationship; the solid line represents the fit of the data with Eq. (4). Right figure: histogram of the residuals R in units of standard deviation [σ] calculated with Eq. (5). The values of R are given in column 7 of Table 1. The solid line represents the fit of the data with a Gaussian

The 2814-keV line of ^{39}K was used to calculate the relative intensities of the other lines which are given together with the values obtained in [5] in Table 4. The relationship between the intensities is shown in Fig. 7 and is expressed by Eq. (4) with $a = 1.24 \pm 0.26$ and $b = 0.89 \pm 0.08$. The Gaussian fit of the histogram of the residuals indicate an agreement between the two data sets at the 1.3σ level. The Gaussian centroid is shifted by 0.11 ± 0.15, reflecting no significant systematic effect. The $\langle \boldsymbol{\sigma}_{E\gamma} \rangle$-values are given in column 4 of Table 4.

Additionally, the 770.3-, 1158.9- and 1618.9-keV rays of the ^{39}K(n, γ)^{40}K reaction were observed in the spectrum. Their production cross sections calculated by Eq. (1) with a neutron total neutron flux of $(1.16 \pm 0.04) \times 10^8$ cm^{-2} s^{-1} are given in Table 5. The relative intensities of the 1158.9- and 1618.9-keV lines calculated using the 770.3-keV line as reference line (100%) are comparable to the intensities derived from the gamma-ray production cross sections for thermal neutron capture $\sigma_{E_\gamma,th}$ (see Table 5). This confirms the fact that the branching ratio of radiative capture lines are independent of the neutron energy as mentioned in our measurements on indium [8] and nickel [11] (Fig. 8).

Gamma rays of oxygen and carbon

The gamma lines induced by the inelastic scattering of fast neutrons on carbon and oxygen were also evaluated and their associated production cross sections calculated by means of Eq. (1). For the 4441-keV line from ^{12}C(n,n′γ)^{12}C, values of 14.8 ± 1.6 mb and 15.6 ± 1.4 mb, were derived from the Na_2CO_3 and the K_2CO_3 spectrum, respectively. Both values agree well with the values deduced from our previous investigations on $CaCO_3$, 14.4 ± 3.3 mb [3] and PVC, 12.8 ± 2.3 mb [9]. The values obtained for the 6129-keV line from ^{16}O(n,n′γ)^{16}O, 2.48 ± 0.33 mb (Na_2CO_3 spectrum), 2.26 ± 0.23 mb (SiO_2 spectrum) and 1.96 ± 0.22 mb (K_2CO_3 spectrum), and for the 1981-keV line from ^{18}O(n,n′γ)^{18}O, 221 ± 30 mb (Na_2CO_3 spectrum), 199 ± 21 mb (SiO_2 spectrum) and 178 ± 30 mb (K_2CO_3 spectrum) match well the values obtained from the measurement of $CaCO_3$ (2.20 ± 0.37 mb and 201 ± 28 mb) [3] and from the measurement of $TbCl_3$ $6H_2O$ (2.22 ± 0.31 mb and 213 ± 40 mb) [10]. Thus, by averaging the aforementioned values we propose following cross sections: 14.4 ± 1.2 mb for the 4441-keV line of ^{12}C, 2.22 ± 0.18 mb for the 6129-keV line of ^{16}O and 202 ± 16 mb for the 1981-keV line of ^{18}O.

Detection limit

The detection limit (DL) corresponding to the smallest quantity of element that can be detected was determined by means of Eq. (1) for a counting time of 12 h, a fast neutron flux of 1.13×10^8 cm^{-2} s^{-1} and from a minimum peak count $\boldsymbol{P}_{E\gamma}(\mathbf{c})$ defined as [28]:

$$P_{E\gamma}(c) = \frac{\sqrt{2 \cdot B_{E\gamma}}}{c} \tag{6}$$

where $\boldsymbol{B}_{E\gamma}$ is the count of the background below the considered gamma line and $c = 0.5$ corresponding to a peak count uncertainty of 50%. In the case of the presence of an interfering line, $\boldsymbol{B}_{E\gamma}$ was replaced by $(2\boldsymbol{B}_{E\gamma} + \boldsymbol{P}_{int})$ in Eq. (6) where $\boldsymbol{P}_{int}$ is the net count of the interfering line. The values of $\boldsymbol{B}_{E\gamma}$ and $\boldsymbol{P}_{int}$ were derived from the beam background

Table 4 Prompt gamma rays induced by fission neutrons on potassium

Reaction	This work				From Demidov Atlas [Ref]		R
	E_γ (keV)	$P_{E_\gamma}/\varepsilon_{E_\gamma}(\times 10^{-8})$ (Count)	I_R(relative) (%)	$\langle\sigma_{E\gamma}\rangle$ (mb)	E_γ (keV)	I_{RD}(relative) (%)	
$^{39}K(n,n'\gamma)^{39}K$	345.84 ± 0.17	0.44 ± 0.07	4.71 ± 0.78	1.28 ± 0.21	346.9 ± 0.3	8.0 ± 1.0	−2.59
	782.88 ± 0.04	1.25 ± 0.06	13.3 ± 0.8	3.63 ± 0.22	783.7 ± 0.5	16 ± 3	−0.87
	923.88 ± 0.28	0.69 ± 0.07	7.38 ± 0.78	2.00 ± 0.21	923.3 ± 0.8	7.2 ± 1.6	0.10
	1129.93 ± 0.09[a]	0.29 ± 0.03	3.10 ± 0.36	0.84 ± 0.09	1129.9 ± 0.5[b]	9 ± 2	−2.90
	1312.60 ± 0.05	1.37 ± 0.06	14.7 ± 0.8	3.98 ± 0.22	1313.3 ± 0.4	12 ± 2	1.25
	1559.79 ± 0.07	0.32 ± 0.10[h]	3.42 ± 1.07	0.93 ± 0.29			
	1573.59 ± 0.13	0.29 ± 0.02	3.10 ± 0.28	0.84 ± 0.06	–	–	–
	1865.29 ± 0.17	0.31 ± 0.03	3.31 ± 0.29	0.90 ± 0.09	1866.6 ± 0.6	3.3 ± 0.8	0.01
	1924.22 ± 0.41	0.19 ± 0.03	2.03 ± 0.33	0.55 ± 0.09	–	–	–
	1951.39 ± 0.29	0.35 ± 0.03	3.74 ± 0.39	1.02 ± 0.09	–	–	–
	2522.37 ± 0.10[c]	6.68 ± 0.21	71 ± 3	19.3 ± 0.9	2522.8 ± 0.3	67 ± 6	0.60
	2814.15 ± 0.09	9.35 ± 0.29	100	27.2 ± 1.3	2813.8 ± 0.4	100	
	3018.79 ± 0.09	3.66 ± 0.12	39 ± 2	10.6 ± 0.5	3018.6 ± 0.8	35 ± 5	0.74
	3597.52 ± 0.12	1.22 ± 0.05	13.0 ± 0.6	3.55 ± 0.19	3596.8 ± 1.2	22 ± 4	−2.22
	3883.50 ± 0.14	1.45 ± 0.07	15.5 ± 0.9	4.22 ± 0.25	3883.1 ± 1.0	20 ± 4	−1.10
	3939.57 ± 0.17	1.02 ± 0.06	10.9 ± 0.7	2.97 ± 0.20	3938.7 ± 1.5	7.5 ± 3.2	1.04
	4083.22 ± 0.17	0.56 ± 0.05	5.99 ± 0.59	1.63 ± 0.16	4083.2 ± 1.2	3.3 ± 1.5	1.67
	4474.98 ± 0.27	0.19 ± 0.02	2.03 ± 0.27	0.55 ± 0.06	–	–	–
	4739.19 ± 0.14	0.40 ± 0.05	4.28 ± 0.55	1.16 ± 0.15	–	–	–
$^{41}K(n,n'\gamma)^{41}K$	578.79 ± 0.14	0.22 ± 0.07	2.35 ± 0.77	8.85 ± 2.83	580.7 ± 1.0	3 ± 1	−0.51
	947.62 ± 0.26	0.11 ± 0.03	1.18 ± 0.27	4.44 ± 1.22	–	–	–
	980.15 ± 0.17	2.98 ± 0.13	32 ± 2	120 ± 7	980.6 ± 0.2	31 ± 5	0.18
	1022.42 ± 0.08	0.39 ± 0.04	4.17 ± 0.47	15.7 ± 1.7	1022.5 ± 1.0	2.5 ± 0.8	1.80
	1186.06 ± 0.17[d]	0.25 ± 0.03	2.67 ± 0.36	10.0 ± 1.2	–	–	–
	1293.36 ± 0.05[e]	2.10 ± 0.26	22 ± 3	82 ± 10	1293.3 ± 0.8	26 ± 6	−0.60
	1418.63 ± 0.22	0.24 ± 0.03	2.57 ± 0.38	9.68 ± 1.26	–	–	–
	1559.79 ± 0.07[f,]	1.32 ± 0.12	14.1 ± 1.3	40 ± 13[g]	1560.1 ± 0.4	11 ± 2	1.25
	1581.82 ± 0.07[i]	0.92 ± 0.09	9.84 ± 0.98	37 ± 4	1580.4 ± 0.8	5 ± 2	2.17
	1592.52 ± 0.12	0.40 ± 0.05	4.28 ± 0.53	16.1 ± 2.1	–	–	–
	1677.0 ± 0.07	1.83 ± 0.20	19.6 ± 2.2	74 ± 8	1676.7 ± 0.4	20 ± 3	−0.11
	1697.38 ± 0.08	1.83 ± 0.23	19.6 ± 2.5	74 ± 10	1698.3 ± 0.4	17 ± 3	0.66
	1920.80 ± 0.56	0.12 ± 0.04	1.28 ± 0.38	4.82 ± 1.48	–	–	–
	2143.50 ± 0.15	0.44 ± 0.07	4.70 ± 0.80	17.7 ± 5.9	–	–	–
	2756.75 ± 0.30	0.25 ± 0.05	2.67 ± 0.29	10.0 ± 2.0	–	-	–
$^{39}K(n,p\gamma)^{39}Ar$	249.92 ± 0.03	1.18 ± 0.12	12.6 ± 1.3	3.43 ± 0.37	250.2 ± 0.4	13 ± 4	−0.10
	985.52 ± 0.11	0.50 ± 0.06	5.35 ± 0.69	1.45 ± 0.18	–	–	–
	1090.57 ± 0.27	0.10 ± 0.03	1.07 ± 0.33	0.29 ± 0.09	–	–	–
	1164.95 ± 0.05[j]	1.16 ± 0.05	12.4 ± 0.7	1.34 ± 0.41[k]	1165.2 ± 0.4	18 ± 2	−2.55
	1266.98 ± 0.05	5.19 ± 0.12	55.5 ± 6.9	15.1 ± 2.2	1267.2 ± 0.2	52 ± 5	0.41
	1517.25 ± 0.06	1.08 ± 0.15	11.6 ± 1.6	3.14 ± 0.49	1517.7 ± 0.3	10 ± 2	0.62
	2092.36 ± 0.08	1.42 ± 0.21	15.2 ± 2.2	4.13 ± 0.68	2092.7 ± 0.6	20 ± 4	−1.05
	2341.93 ± 0.10 [m]	0.57 ± 0.10	6.10 ± 1.04	1.66 ± 0.31	2343.2 ± 0.6	7.2 ± 1.5	−0.60
	2433.8 ± 1.4	0.16 ± 0.05	1.71 ± 0.54	0.46 ± 0.14	–	–	–
	2481.54 ± 0.14[n]	0.55 ± 0.09	5.88 ± 1.00	1.60 ± 0.35	2481.5 ± 1.0	7.2 ± 2.5	−0.49
	2650.03 ± 0.11	0.42 ± 0.09	4.49 ± 0.93	1.22 ± 0.27	–	–	–
	3061.47 ± 0.11	0.32 ± 0.05	3.42 ± 0.54	0.93 ± 0.16	–	–	–

Table 4 (continued)

Reaction	This work				From Demidov Atlas [Ref]		R
	E_γ (keV)	$P_{E_\gamma}/\varepsilon_{E_\gamma}(\times 10^{-8})$ (Count)	I_R(relative) (%)	$\langle\sigma_{E\gamma}\rangle$ (mb)	E_γ (keV)	I_{RD}(relative) (%)	
^{39}K(n,αγ)^{36}Cl	787.92 ± 0.04	1.75 ± 0.11	18.7 ± 2.2	5.09 ± 0.70	788.5 ± 0.5	22 ± 3	− 0.89
	1164.95 ± 0.05	0.68 ± 0.16[l]	7.28 ± 1.67	1.97 ± 0.44			

E_γ is the gamma-ray energy, $P_{E_\gamma}/\varepsilon_{E_\gamma}$ the net count in the gamma-ray peak divided by the full-energy-peak efficiency and the gamma-ray self-absorption factor,I_R the relative intensity of the gamma-ray and $\langle\sigma_{E\gamma}\rangle$ the fast neutron spectrum averaged isotopic cross section for gamma ray production at an angle of 90° between neutron beam and detector determined with Eq. (1). R is the residual calculated by means of Eq. (6). The uncertainty for $P_{E\gamma}(90°)/(\varepsilon_{E\gamma}{\cdot}f_{E\gamma})$ is calculated from the uncertainty of the net counts of the lines $P_{E\gamma}(90°)$ and the uncertainty of the full-energy peak efficiency $\varepsilon_{E\gamma}$ (3%) The uncertainty for $<\sigma_{E\gamma}(90°)>$ is calculated from the uncertainty of $P_{E\gamma}(90°)/(\varepsilon_{E\gamma}{\cdot}f_{E\gamma})$ and the uncertainty of the fast neutron flux (3.5%)

[a]Corrected for the contribution of the 1130-keV (^{74}Ge) background line (43.5% of total counts)

[b]Possible interference of the 1130-keV line probably not considered

[c]Corrected for the contribution of the 2522-keV (^{70}Ge, ^{72}Ge) background line (3.2% of total counts)

[d]Corrected for the contribution of the single escape peak of the 1697-keV (^{41}K) line (13% of total counts)

[e]Corrected for the contribution of the 1293-keV (^{41}Ar) line (1.6% of total counts)

[f]Contains a contribution of the 1559-keV line of ^{39}K

[g]Calculated with $P_{E_\gamma}/\varepsilon_{E_\gamma} = (1.00 \pm 0.32)\ 10^8$ obtained using an intensity ratio of 4.54 between 1559- and 579-kev lines of ^{41}K [21]

[h]Corrected from the contribution of the 1559-keV line of ^{41}K. See note g

[i]Corrected for the contribution of the single escape peak of the 2092-keV (^{41}Ar) line (7.2% of total counts)

[j]Corrected for the contribution of the single escape peak of the 1677-keV (^{41}K) line (2.2% of total counts). Contains a contribution of the 1165-keV line of ^{36}Cl

[k]Calculated with $P_{E_\gamma}/\varepsilon_{E_\gamma} = (0.46 \pm 0.14)\ 10^8$ obtained using an intensity ratio of 2.91 between 1165- and 2433-kev lines of ^{39}Ar [20]

[l]Corrected from the contribution of the 1165-keV line of ^{39}Ar. See note k

[m]Could contain a contribution of the 2343-kev line of ^{39}K

[n]Could contain a contribution of the 2481-kev line of ^{41}K

Table 5 Prompt gamma rays induced by radiative capture in ^{39}K

Reaction	This work				Capture of thermal neutrons [Ref]	
	Eγ (keV)	$P_{E_\gamma}/\varepsilon_{E_\gamma}$ ($\times 10^{-8}$) (Count)	I_R(relative) (%)	$\sigma_{E\gamma}$ (mb)	$\sigma_{E\gamma,th}$ (mb)	$I_{E\gamma,th}$(relative) (%)
^{39}K(n,γ)^{40}K	770.3	0.76 ± 0.03	100	2.15 ± 0.11	968 ± 13	100
	1158.9	0.13 ± 0.04	17.1 ± 5.3	0.38 ± 0.12	171.7 ± 2.7	17.7 ± 0.4
	1618.9	0.12 ± 0.03	15.8 ± 3.9	0.34 ± 0.09	139.4 ± 2.2	14.4 ± 0.3

Eγ is the gamma-ray energy, $P_{E_\gamma}/\varepsilon_{E_\gamma}$ the net count in the gamma-ray peak divided by the full-energy-peak efficiency and the gamma-ray self-absorption factor,I_R the relative intensity of the gamma ray and $\langle\sigma_{E\gamma}\rangle$ the fast neutron spectrum averaged isotopic cross section for gamma ray production determined with Eq. (1). $\sigma_{E\gamma,th}$ is the production cross section and $I_{E\gamma,th}$ the relative intensity of the gamma ray for thermal neutron capture

spectrum. The DL obtained for sodium, silicon, sulfur and potassium are 0.1 mg (^{23}Na, $E_\gamma = 439.4$ keV, $\langle\boldsymbol{\sigma_{E\gamma}}\rangle =$ 507 mb), 0.6 mg (^{28}Si, $E_\gamma = 1778.8$ keV, $\langle\boldsymbol{\sigma_{E\gamma}}\rangle = 189$ mb), 1 mg (^{32}S, $E_\gamma = 2230.5$ keV, $\langle\boldsymbol{\sigma_{E\gamma}}\rangle = 79$ mb) and 4 mg (^{39}K, $E_\gamma = 2814.1$ keV, $\langle\boldsymbol{\sigma_{E\gamma}}\rangle = 27.2$ mb).

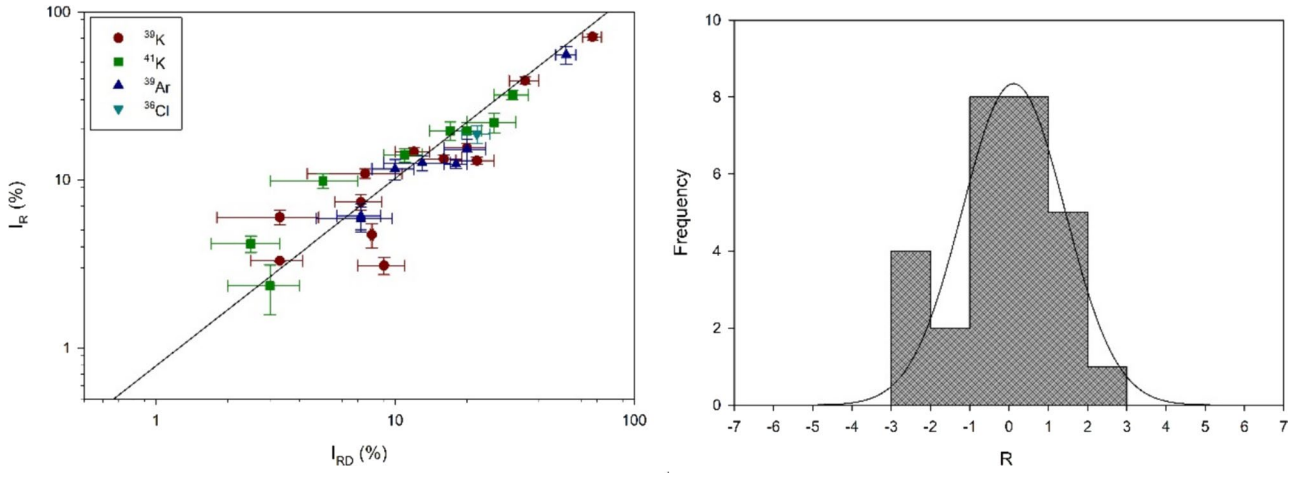

Fig. 8 Comparison of the relative intensities of the prompt gamma rays induced by fission neutrons on potassium obtained in this work with the data tabulated in the Demidov Atlas [5]. Left figure: linear relationship; the solid line represents the fit of the data with Eq. (4). Right figure: histogram of the residuals R in units of standard deviation [σ] calculated with Eq. (5). The values of R are given in column 7 of Table 1. The solid line represents the fit of the data with a Gaussian

Conclusions

The emission of prompt gamma rays induced by (n,n′γ)-reactions on sodium and by (n,n′γ)-, (n,pγ)-, (n,$\alpha\gamma$)-reactions on silicon, sulfur and potassium was investigated with the FaNGaS instrument by irradiating Na_2CO_3, SiO_2, S and K_2CO_3 samples with fission neutrons. A total of 19, 13, 20 and 48 prompt gamma lines were observed for sodium, silicon, sulfur and potassium, respectively and their relative intensities and partial production cross sections determined. Compared with [5], 24 lines were detected additionally (1 for sodium, 1 for silicon, 5 for sulfur and 17 for potassium), all being mentioned in NuDat 3.0 [4]. The relative intensities of the lines were found to agree reasonably (0.6σ level for sodium, 0.9σ level for silicon, 1.5σ level for sulfur and 1.3σ level for potassium) with the values given in [5]. The detection limits of sodium, silicon, sulfur and potassium are 0.1, 0.6, 1 and 4 mg, respectively, for a counting time of 12 h and a neutron flux of 1.13×10^8 cm^{-2} s^{-1}. In addition, the partial cross section for production of the carbon and oxygen lines from inelastic scattering reactions were found to match well the values determined in our previous works [3, 9, 10].

Author contributions The 5th. author, Zsolt Révay is a member of the Editorial Board of the journal. Therefore, he did not take part in the review process in any capacity and the submission was handled by a different member of the editorial board.

Funding Open Access funding enabled and organized by Projekt DEAL.

Data availability Data sets generated during the current study are available from the corresponding author on reasonable request.

Declarations

Conflict of interest The authors declare that they have no conflict of interest.

References

1. Randriamalala TH, Rossbach M, Mauerhofer E, Zs R, Söllrad S, Wagner FM (2016) FaNGaS: a new instrument for (n, n´, γ) reaction measurements at FRM II. Nucl Instrum Meth A806:370–377
2. Ilic Z, Mauerhofer E, Stieghorst C, Zs R, Rossbach M, Randriamalala TH, Brückel T (2020) Prompt gamma rays induced by inelastic scattering of fission neutrons on iron. J Radioanal Nucl Chem 325:641–645
3. Ophoven N, Ilic Z, Mauerhofer RTH, Vezhlev E, Stieghorst C, Zs R, Brückel T, Jolie J, Strub E (2022) Fast neutron induced gamma rays from (n, n´), (n, p) and (n, α) reactions on $CaCO_3$. J Radioanal Nucl Chem 331:5729–5740
4. NuDat 3.0 National Nuclear Data Center, Brookhaven National Laboratory https://www.nndc.bnl.gov/nudat3/
5. Demidov A, Govor L, Cherepantsev M, Ahmed S, Al-Najiar M, Al-Amili N, Al-Assafi N, Rammo N (1978) Atlas of gamma-ray

spectra from the inelastic scattering of reactor fast neutrons. Atomizdat, Moscow
6. Hurst AM, Bernstein LA, Kawano T, Lewis AM, Song K (2021) The Baghdad atlas: a relational database of inelastic neutron scattering (n, n´γ) data. Nucl Instrum Meth A 995:165095
7. Mauerhofer E, Ilic Z, Stieghorst C, Zs R, Vezhlev E, Ophoven N, Randriamalala TH, Brückel T (2022) Prompt gamma rays from fast neutron inelastic scattering on aluminum, titanium and copper. J Radioanal Nucl Chem 331:3987–4000
8. Mauerhofer E, Ilic Z, Stieghorst C, Zs R, Rossbach M, Li J, Randriamalala TH, Brückel T (2021) Prompt and delayed gamma rays induced by epithermal and fast neutrons with indium. J Radioanal Nucl Chem 331:535–546
9. Ophoven N, Ilic Z, Mauerhofer E, Randriamalala TH, Vezhlev E, Stieghorst C, Zs R, Brückel T, Jolie J, Strub E (2023) Prompt gamma rays from fast neutron induced reactions on cerium and chlorine. J Radioanal Nucl Chem 332:3133–3145
10. Ophoven N, Ilic Z, Mauerhofer E, Randriamalala TH, Vezhlev E, Stieghorst C, Zs R, Jolie J, Strub E (2024) Prompt gamma rays of terbium induced by inelastic scattering of fission neutrons. J Radioanal Nucl Chem 332:3133–3145
11. Mauerhofer E, Ophoven N, Ilic Z, Stieghorst C, Zs R, Meleshenkovskii I, Randriamalala TH (2024) Gamma emission from interaction of fission neutrons on nickel and zirconium. J Radioanal Nucl Chem 333:4333–4352
12. Ophoven N, Mauerhofer E, Ilic Z, Stieghorst C, Zs R, Meleshenkovskii I, Randriamalala TH (2024) Prompt gamma rays of lanthanum and praseodymium produced by inelastic scattering of fission neutrons. J Radioanal Nucl Chem. https://doi.org/10.1007/s10967-024-09821-y
13. Zs R, Belgya T, Molnár GL (2005) Application of Hypermet-PC in PGAA. J Radioanal Nucl Chem 265:261–265
14. Shamsuzzoha Basunia M, Chakraborty A (2021) Nuclear data sheets for A = 23. Nucl Data Sheets 171:1–252
15. Shamsuzzoha Basunia M (2013) Nuclear data sheets for A = 28. Nucl Data Sheets 114:1189–1291
16. Shamsuzzoha Basunia M (2012) Nuclear data sheets for A = 29. Nucl Data Sheets 113:909–972
17. Shamsuzzoha Basunia M, Chakraborty A (2024) Nuclear data sheets for A = 30. Nucl Data Sheets 197:1–258
18. Ouellet C, Singh B (2011) Nuclear data sheets for A = 32. Nucl Data Sheets 112:2199–2355
19. Nica N, Singh B (2012) Nuclear data sheets for A = 34. Nucl Data Sheets 113:1563–1733
20. Chen J (2018) Nuclear data sheets for A = 39. Nucl Data Sheets 149:1–251
21. Nesaraja CD, McCutchan EA (2016) Nuclear data sheets for A = 41. Nucl Data Sheets 133:1–220
22. Révay Z, Firestone RB, Belgya T, Molnár GL (2004) Prompt gamma-ray spectrum catalog. In: Molnár GL (ed) Handbook of prompt gamma activation analysis. Springer US, Boston, MA, pp 173–364
23. Brown DA et al (2018) ENDF/B-VIII.0: the 8th major release of the nuclear reaction data library with CIELO-project cross sections, new standards and thermal scattering data. Nucl Data Sheets 148:1–142
24. MacFarlane RE, Kahler AC (2010) Methods for processing ENDF/B-VII with NJOY. Nucl Data Sheets 111:2739–2890
25. MacFarlane R, Muir DW, Boicourt RM, Kahler AC, Conlin JL (2017) The NJOY Nuclear Data Processing System, Version 2016. https://doi.org/10.2172/1338791
26. OECD NEA Data Bank, JANIS Book of neutron-induced cross-sections (2020) https://www.oecd-nea.org/janis/book/book-neutron-2020-09.pdf
27. NIST XCOM: Photons Cross Sections Database, National Institute of Standards and Technology https://physics.nist.gov/PhysRefData/Xcom/html/xcom1.html
28. Zs R (2009) Determining elemental composition using prompt γ activation analysis. Anal Chem 81:6851–6859